RSC Advances

PAPER

Cite this: *RSC Adv.*, 2015, **5**, 52958

Effects of alkaline-earth oxides on the performance of a CuO–ZrO_2 catalyst for methanol synthesis *via* CO_2 hydrogenation

Chenglin Zhong, Xiaoming Guo,* Dongsen Mao, Song Wang, Guisheng Wu and Guanzhong Lu

Received 11th April 2015
Accepted 10th June 2015

DOI: 10.1039/c5ra06508a

www.rsc.org/advances

CuO–ZrO_2 catalysts doped with alkaline-earth oxides were prepared by a urea-nitrate combustion method. The catalysts were characterized with N_2 adsorption, N_2O titration, XRD, H_2-TPR, XPS and CO_2-TPD techniques and tested for methanol synthesis from CO_2 hydrogenation. With the incorporation of alkaline-earth oxides, the copper surface area increases remarkably, whereas the reducibility of CuO in the catalyst decreases. The doping of alkaline-earth oxides leads to an increase in the strength and contribution of the strong basic site on the catalyst surface. The results of catalytic tests indicate that the conversion of CO_2 depends not only on the copper surface area but also on the reducibility of CuO in the catalyst, and the latter is a predominant factor for CaO-, SrO- and BaO-doped CuO–ZrO_2 catalysts. The selectivity to methanol is related to the basicity of the catalyst. Moreover, the influence of the doping amount of MgO on the properties of CuO–ZrO_2 was investigated, and the optimum catalytic activity is obtained as the amount of MgO doping is 5 mol%.

1. Introduction

Carbon dioxide has been widely regarded as the main greenhouse gas, linked to the problem of global warming. Carbon dioxide is also available as an infinite carbon source. Efficient conversion of carbon dioxide is of great significance from the viewpoint of environmental protection and effective utilization of carbon resources. Most of the existing research focuses on CO_2 hydrogenation to methanol since methanol is an important feedstock for the organic chemical industry and a potential alternative to fossil fuels.[1,2] Based on the great significance of methanol synthesis from CO_2 hydrogenation, the concept of "methanol economy" was proposed by Nobel laureate Olah.[3]

It is well documented that CuO–ZrO_2 based catalysts exhibit a high catalytic activity for methanol synthesis from CO_2 hydrogenation.[4–9] To further improve the performance of CuO–ZrO_2 based catalyst, a variety of promoters were added, and the effects of these promoters were estimated.[10–14] For example, Kilo *et al.*[10] studied the effects of Cr and Mn oxide on the structural and catalytic properties of CuO–ZrO_2. They found that the presence of Cr or Mn retarded the sintering of copper crystallite and stabilized the amorphous state of zirconia, thus resulting in an increased thermal stability of catalysts. Słoczyński *et al.*[11,12] investigated a series of CuO–ZnO–ZrO_2 catalysts promoted by B, Mn, Mg and Ga, and the results showed that the promoters modified the dispersion of Cu (or the copper surface area), the surface composition of catalyst and the catalytic activity for methanol synthesis. Natesakhawat *et al.*[13] found that the incorporation of Ga_2O_3 and Y_2O_3 into CuO–ZnO–ZrO_2 catalysts enhanced the Cu dispersion and the reducibility of CuO, and a superior methanol synthesis activity was obtained over the doped catalysts. These studies focused on the influences of promoters on the properties of Cu component in catalysts. However, some researches revealed that there were two active centers involved in the catalytic process of CO_2 hydrogenation over the Cu/ZrO_2-based catalysts.[15–17] One is the Cu component, and the other is the so-called "support" ZrO_2. The Cu serves to dissociatively adsorb H_2 and to provide a source of atomic hydrogen by spillover, and the ZrO_2 serves to adsorb CO_2 as carbonate-like species which then undergo stepwise hydrogenation to methanol. Such a mechanism is known as "dual-site" mechanism, and it is currently accepted. Because CO_2 is intrinsically an acid molecular, the adsorption and the activation of CO_2 are related closely to the surface basicity of ZrO_2. In our previous work,[18] the influence of La doping on the catalytic behavior of CuO–ZrO_2 for methanol synthesis was investigated. The results indicate that the conversion of CO_2 depends on the copper surface area, whereas the selectivity to methanol is related to the distribution of basic site on the catalyst surface. Recently, Gao *et al.* studied a series of promoted CuO–ZnO–Al_2O_3 catalyst derived from the hydrotalcite-like precursors, and similar results were presented.[19,20] Therefore, both the copper surface area and the surface basicity should be taken into consideration when

Research Institute of Applied Catalysis, School of Chemical and Environmental Engineering, Shanghai Institute of Technology, Shanghai 200235, P. R. China. E-mail: guoxiaoming@sit.edu.cn; Fax: +86-21-60873301; Tel: +86-21-60873301

selecting a suitable promoter for catalyst. Alkaline-earth oxide, a well-known solid base, has been employed in a variety of organic reactions as the main component or promoter of catalyst.[21] Moreover, alkaline-earth oxide exhibits a high thermal stability, which can prevent the agglomeration of catalyst and increase the surface area of catalyst.[22,23] Thus, the introduction of alkaline-earth oxide into CuO–ZrO_2 may regulate the surface basicity and improve the Cu dispersion of catalysts. However, to date, a systematic examination of CuO–ZrO_2 catalyst doped with alkaline-earth oxides for CO_2 hydrogenation is absent.

The primary purpose of the present work is to explore the influence of alkaline-earth oxides (MgO, CaO, SrO and BaO) doping on the properties of CuO–ZrO_2 catalysts. The physicochemical properties of alkaline-earth oxides doped CuO–ZrO_2 catalysts were characterized by XRD, BET, N_2O titration, TPR, XPS and CO_2-TPD techniques, and the catalytic activity for methanol synthesis from CO_2 hydrogenation was evaluated. Based on the catalytic mechanism of methanol synthesis, the catalytic activity and selectivity of the doped catalysts were discussed in relation to the physicochemical properties including the copper surface area, the reducibility of CuO and the surface basicity. In addition, the effects of doping amount was emphasized for MgO-doped catalyst.

2. Experimental

2.1 Catalyst preparation

CuO–ZrO_2 (CZ) and alkaline-earth oxides doped CuO–ZrO_2 (MCZ, M = Mg, Ca, Sr, Ba) catalysts were prepared by the urea-nitrate combustion method. All chemicals used were of analytical reagent grade (Shanghai Chemical Reagent Corporation, Shanghai, China). Firstly, the required amounts of metal nitrates were dissolved in deionized water in a basin to form a mixed solution with a total cation concentration of 3.0 M. Then, the solution of urea (3.5 M) was slowly added to the metal nitrate solution under constant stirring. The resulting mixture was kept in an ultrasound bath operating at 47 kHz with a power of 30 W for 0.5 h until a pale-blue slurry was obtained. Afterward, the slurry was transferred to an open muffle furnace preheated at 300 °C. The slurry started boiling with frothing and foaming, and ignition took place. Along with rapid evolution of a large quantity of gases, a foamy, voluminous powder was produced. Because the time for the autoignition was rather short, to remove traces of undecomposed urea, nitrates and their decomposition products, the powder was further calcined in air at 500 °C for 4 h. To obtain an optimum catalytic performance, the amount of urea used in the combustion process was 50% of the stoichiometric amount, which can be calculated according to propellant chemistry.[24] A more detailed description of the preparation process was given in ref. 8. Unsupported CuO powder in this study was prepared *via* the thermal decomposition of $Cu(NO_3)_2$ at 500 °C. The synthesized catalysts are denoted as $M_xC_yZ_z$, where x, y and z represent the atomic concentration of alkaline-earth metal, Cu and Zr, respectively. The sum of atomic concentration of metal was taken as 1.0, and a constant atomic concentration of Cu (0.5) was employed in this study.

2.2 Catalyst characterization

The X-ray diffraction (XRD) analysis of the sample was carried out on a PANalytical X'Pert diffractometer using nickel-filtered Cu Kα radiation at 40 kV and 40 mA. Two theta angles ranged from 10 to 70° with a speed of 6° per minute.

The BET surface area (S_{BET}) of sample was determined by a Micromeritics ASAP2020M + C adsorption apparatus with nitrogen adsorption/desorption isotherms. Before each analysis, samples were dried at 200 °C under vacuum for 3 h.

Copper surface area (S_{Cu}) in the reduced catalyst was determined using the N_2O titration method similar to that described by Chinchen *et al.*[25] The catalyst (0.2 g) was reduced in an H_2/He mixture at 300 °C for 1 h. Then, it was purged with He and cooled to 60 °C. A flow of 1 vol% N_2O/He gas mixture was fed into the reactor. The N_2 produced by the decomposition of N_2O on the exposed Cu atoms was detected using a mass spectrometer (Pfeiffer Vacuum Quadstar, 32-bit). The copper surface area was calculated assuming an atomic copper surface density of 1.46×10^{19} Cu atoms per m^2 and a molar stoichiometry of $N_2O/Cu = 0.5$.[7]

Temperature-programmed reduction (TPR) measurements were performed in a linear quartz microreactor fed with a 10 vol% H_2/N_2 mixture flowing at 50 ml min^{-1} and heated at a rate of 5 °C min^{-1}. A *ca.* 30 mg of a freshly calcined catalyst was placed on top of glass wool in the reactor. The outlet of the reactor was connected to a glass column packed with molecular sieve 5 Å in order to remove the moisture produced from reduction. The amount of consumed H_2 was measured by a thermal conductivity detector (TCD).

The surface electronic states were investigated by X-ray photoelectron spectroscopy (XPS, ESCALAB 250Xi, Thermo Scientific Escalab) with Al Kα (1486.6 eV) radiation as the X-ray excitation source. All the binding energy values were calibrated by using C 1s = 284.8 eV as a reference.

The basicity of the catalysts was measured by CO_2 temperature-programmed desorption (CO_2-TPD). Prior to the adsorption of CO_2, the catalysts were reduced at 300 °C for 60 min in a flow of 10% H_2/N_2 mixture. After cooling to room temperature, the catalyst was saturated with CO_2 at 50 °C for 60 min, and then flushed with He flow to remove any physisorbed molecules. Afterward, the TPD experiment was started with a heating rate of 5 °C min^{-1} under He flow, and the desorbed CO_2 was detected by a mass spectrometer. The amount of the desorbed CO_2 was quantified by comparing the integrated area of the TPD curves to the peak area of the injected CO_2 calibration pulse.

2.3 Catalytic testing

Catalytic activity and selectivity tests for methanol synthesis from CO_2 hydrogenation were carried out in a continuous-flow, fixed-bed reactor. Prior to the catalytic measurements, the fresh catalyst was reduced in a stream of 10 vol% H_2/N_2 at 300 °C for 3 h under atmospheric pressure. Then the reactor was cooled to 180 °C and the reactant gas ($CO_2 : H_2 = 1 : 3$, molar) flow was introduced, raising the pressure to 3.0 MPa and the temperature to a given temperature. The transfer line from the reactor to

the chromatograph was heated at 140 °C in order to avoid condensation of the reaction products. Effluent products were analyzed on-line with a gas chromatograph (6820, Agilent). The gases CO_2, CO and the internal standard N_2 were analyzed using a thermal conductivity detector (TCD); organic products were analyzed with a flame ionization detector (FID). Conversion and selectivity values were calculated by mass-balance methods and the steady-state values were quoted as the average of four different analyses taken after 5 h on stream operation.

3. Results and discussion

3.1 Textural and structural properties of the catalysts

The XRD spectra of CuO–ZrO_2 catalysts doped with different alkaline-earth oxides (5 mol%) were shown in Fig. 1(A). The diffraction peaks at 2θ of 35.6° and 38.8° are ascribed to the CuO phase (JCPDS 80-1268), and the diffraction peak of 2θ = 30.3° is assigned to the tetragonal ZrO_2 (t-ZrO_2, JCPDS, 88-1007). Furthermore, two small peaks for monoclinic ZrO_2 (m-ZrO_2, 2θ = 28.2°, 31.5°, JCPDS 83-0940) can be detected on the undoped CuO–ZrO_2 sample. With the introduction of alkaline-earth oxides, the diffraction peaks of CuO and t-ZrO_2 become weaker and broader, which indicates that the alkaline-earth oxides hinder the crystallization of CuO and ZrO_2 in catalysts, and such an effect increases in the order MgO < CaO < SrO < BaO. The average particle size of CuO was calculated with Scherer equation. As can be seen from Table 1, the particle size of CuO decreases progressively from MgO-doped to BaO-doped sample. There is no diffraction peaks of alkaline-earth oxides crystallites for all the investigated samples, as shown in Fig. 1(A). The reason for this is ascribed to the formation of non-crystalline $MZrO_3$ (M = Mg, Ca, Sr, Ba) compound, which could not be detected by XRD technique due to the low degree of crystallization. The crystalline $MZrO_3$ compounds can be detected with a high calcination temperature for the samples.[26]

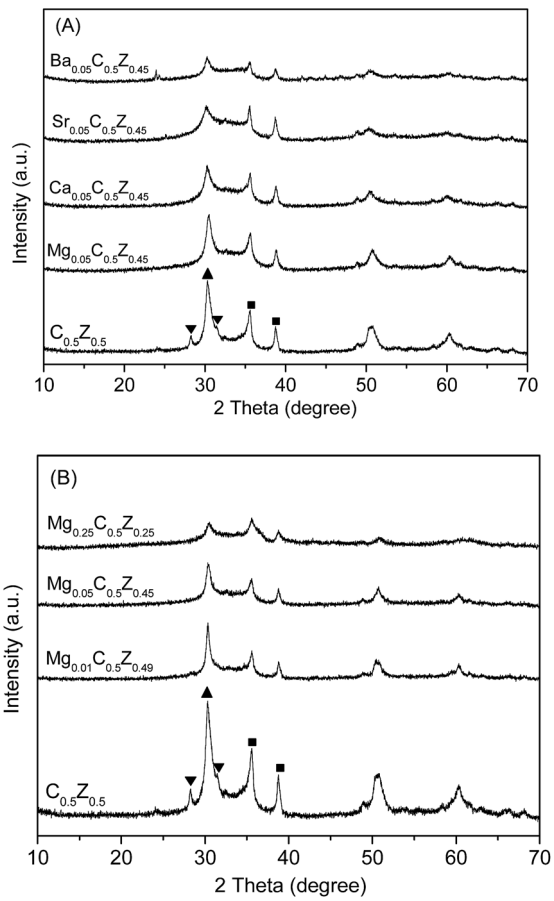

Fig. 1 XRD patterns of CuO–ZrO_2 catalysts doped with different alkaline-oxide (A) and with different amount of MgO (B). (■) CuO; (▲) ZrO_2 (tetragonal); (▼) ZrO_2 (monoclinic).

Fig. 1(B) shows the XRD patterns of CuO–ZrO_2 catalysts with different MgO contents. It can be seen that the diffraction peak intensity of CuO and ZrO_2 decline with increasing MgO concentration. A similar variation trend was observed for the average particle size of CuO, as shown in Table 1. An enlarged view of the diffraction peaks of CuO and ZrO_2 components in MgO-doped CuO–ZrO_2 catalyst was presented in Fig. 2. With the introduction of MgO, the diffraction peak of t-ZrO_2 shifts toward higher 2θ angle. This is an indicative of a decrease in the crystal lattice parameter, which is resulted from the substitution of Zr^{4+} (radius 0.72 Å) by Mg^{2+} cations (radius 0.65 Å).[27] However, there is no shift of CuO diffraction peak after MgO doping. These results further confirmed that Mg^{2+} was incorporated into ZrO_2 lattice rather than CuO lattice.

The BET surface areas derived from nitrogen physisorption are listed in Table 1. A marked increase in S_{BET} was observed for MgO-doped CuO–ZrO_2 catalyst, whereas the increase was not notable for CaO-, SrO-, and BaO-doped samples. Copper surface area, which is determined by N_2O titration, is also presented in Table 1. Obviously, the incorporation of alkaline-earth oxides lead to an increase in S_{Cu} in the order MgO < CaO < SrO < BaO. In the case of MgO-doped samples, the value of S_{Cu} increases continually with increasing MgO doping content, and a maximum of 15.2 $m^2\ g^{-1}$ is obtained over $Mg_{0.25}C_{0.5}Z_{0.25}$ sample. The variation of S_{Cu} is in accordance with the results regarding CuO crystallite size, as determined from XRD.

Table 1 Physicochemical properties of the CuO–ZrO_2 catalysts doping with alkaline-earth oxides

Sample	S_{BET} ($m^2\ g^{-1}$)	CuO crystallite size[a] (nm)	S_{Cu}[b] ($m^2\ g^{-1}$)
$C_{0.5}Z_{0.5}$	35.7	22.9	2.8
$Mg_{0.05}C_{0.5}Z_{0.45}$	45.8	21.0	7.4
$Ca_{0.05}C_{0.5}Z_{0.45}$	37.8	20.8	8.0
$Sr_{0.05}C_{0.5}Z_{0.45}$	37.1	20.8	8.3
$Ba_{0.05}C_{0.5}Z_{0.45}$	36.4	20.3	10.6
$Mg_{0.01}C_{0.5}Z_{0.49}$	39.1	21.7	4.4
$Mg_{0.03}C_{0.5}Z_{0.47}$	45.3	21.2	6.2
$Mg_{0.1}C_{0.5}Z_{0.4}$	46.4	21.2	13.7
$Mg_{0.25}C_{0.5}Z_{0.25}$	56.2	16.2	15.2

[a] Determined by XRD. [b] Determined by N_2O titration at 60 °C.

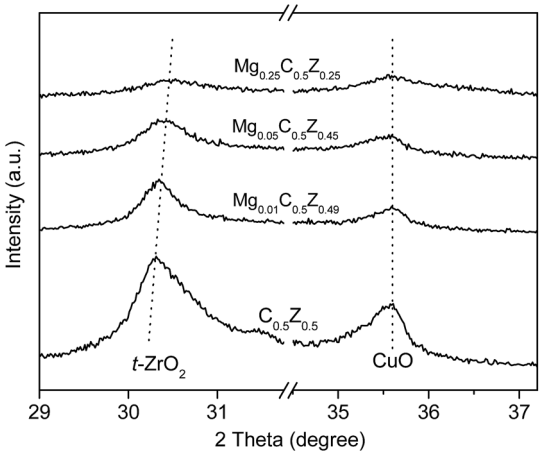

Fig. 2 Magnification XRD patterns of t-ZrO_2 and CuO phase in CuO–ZrO_2 catalysts with different MgO contents.

3.2 The surface oxidation states of catalyst

The surface oxidation states of CuO–ZrO_2 and alkaline-earth oxides doped CuO–ZrO_2 catalysts were investigated by XPS. As shown in Table 2, the binding energies (BE) of Cu $2p_{3/2}$ are in the range of 933.7–934.2 eV for all the catalysts, suggesting that the chemical state of copper is Cu^{2+}.[18] With the introduction of alkaline-earth oxide, a slight shift towards lower BE of Cu $2p_{3/2}$ was observed. The BE value of *ca.* 181.8 eV measured for Zr $3d_{5/2}$ indicates the presence of zirconium oxide with an oxidation state of +4.[11] There is no significant change in the BE value of Zr with the incorporation of alkaline-earth oxide. Furthermore, the BE values of alkaline-earth metal (Mg, Ca, Sr and Ba) in the catalysts are very close to those of the corresponding oxide (MgO, CaO, SrO and BaO), which discloses that the alkaline-earth metal exist in a cationic state.[11,28]

3.3 The reducibility of catalyst

In order to investigate the reduction behavior of the catalysts, H_2-TPR measurements were carried out. Fig. 3(A) shows the TPR profiles of CuO–ZrO_2 catalysts doped with different alkaline-earth oxides. For comparison, the TPR profile of the unsupported CuO powder is also presented. All samples exhibit two reduction peaks, with the exception of MgO-doped CuO–ZrO_2 catalyst. As well documented, the low temperature peak (α peak) is attributed to the reduction of highly dispersed CuO surface species, and the peak appearing at higher temperature (β peak) is due to the reduction of bulk-like CuO.[7,29,30] In addition, as shown in Fig. 3(A), the reduction temperature of CuO in $C_{0.5}Z_{0.5}$ sample is much lower than that of the unsupported CuO (*ca.* 285 °C). This result reveals that ZrO_2 can facilitate the reduction of CuO *via* the interaction between them, a fact that is consistent with previous observations.[31–34] Table 3 summaries the temperatures of reduction peaks for the investigated catalysts. Compared with the undoped CuO–ZrO_2 sample, both α and β peak shift toward higher temperature with the introduction of CaO, SrO and BaO. This indicates that the incorporation of alkaline-earth oxides weakens the interaction between CuO and ZrO_2, which results in a decrease in the reducibility of CuO. As far as the MgO-doped CuO–ZrO_2 catalyst is concerned, the peak appearing in the higher-temperature region splits into two parts, which are denoted as β and γ peak. A similar observation of the multiple TPR peaks for the bulk-like CuO was reported by Wang *et al.*[32] The split of the reduction peak is originated from the difference in the interaction strength, and γ peak corresponds to the reduction of CuO interacting with ZrO_2 weakly. As shown in Table 3, the temperature of reduction peak of MgO-doped catalyst is much lower than that of SrO- and BaO-doped samples. For example, the temperature of β peak of $Sr_{0.05}C_{0.5}Z_{0.45}$ is 234 °C; while that of β and γ peak are 208 and

Table 2 Binding energies of the core electrons for CZ and MCZ (M = Mg, Ca, Sr and Ba) catalysts determined by XPS

	Binding energy (eV)		
Catalyst	Cu $2p_{3/2}$	Zr $3d_{5/2}$	M
CZ	934.2	181.9	—
$Mg_{0.05}C_{0.5}Z_{0.45}$	934.0	181.8	Mg 1s: 1304.8
$Ca_{0.05}C_{0.5}Z_{0.45}$	933.8	181.8	Ca $2P_{3/2}$: 346.9
$Sr_{0.05}C_{0.5}Z_{0.45}$	933.7	181.8	Sr $3d_{5/2}$: 133.2
$Ba_{0.05}C_{0.5}Z_{0.45}$	933.7	181.8	Ba $3d_{5/2}$: 780.1

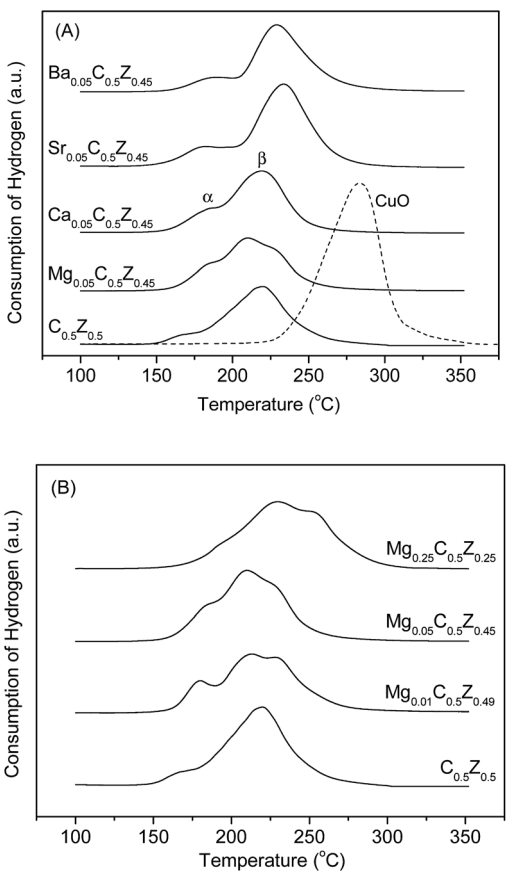

Fig. 3 H_2-TPR profiles of CuO–ZrO_2 catalysts doped with different alkaline-oxide (A) and with different amount of MgO (B).

Table 3 Temperature of reduction peaks over $CuO–ZrO_2$ catalysts doping with alkaline-earth oxides

Catalyst	T_α (°C)	T_β (°C)	T_γ (°C)
$C_{0.5}Z_{0.5}$	175	220	—
$Mg_{0.05}C_{0.5}Z_{0.45}$	183	208	228
$Ca_{0.05}C_{0.5}Z_{0.45}$	185	219	—
$Sr_{0.05}C_{0.5}Z_{0.45}$	186	234	—
$Ba_{0.05}C_{0.5}Z_{0.45}$	190	229	—
$Mg_{0.01}C_{0.5}Z_{0.49}$	179	213	228
$Mg_{0.25}C_{0.5}Z_{0.25}$	205	229	253

228 °C for $Mg_{0.05}C_{0.5}Z_{0.45}$, respectively. These results suggest that a smaller effect of doping on the reducibility of CuO is obtained for the MgO-doped $CuO–ZrO_2$ catalyst.

Fig. 3(B) shows the influence of MgO content on the reduction behavior of $CuO–ZrO_2$ catalyst. The change in the reduction temperature of CuO is insignificant from $Mg_{0.01}C_{0.5}Z_{0.49}$ to $Mg_{0.05}C_{0.5}Z_{0.45}$ sample. However, as the content of MgO reached 25 mol%, the increase in the reduction temperature become distinct. The variation of reduction temperature is also related to the interaction between CuO and ZrO_2, which decreases drastically when excessive MgO is added.

3.4 The basicity of the catalysts

The surface base properties of catalysts were investigated by CO_2-TPD technique, and the CO_2 desorption profiles obtained for $CuO–ZrO_2$ and alkaline-earth oxides doped $CuO–ZrO_2$ catalysts are presented in Fig. 4(A). A desorption peak with a maximum at *ca.* 105 °C was observed for all investigated samples. However, the TPD profile is highly asymmetric with a tail towards higher temperature, which is the result of a complex overlapping of several CO_2 desorption processes arising from different basic sites. In general, the basicity of metal oxide can be divided into three categories (weak, medium, and strong) according to the strength of base site.[35,36] The weak basic sites are related to the surface hydroxyl group; the medium basic sites are ascribed to the metal–oxygen pairs, *i.e.* Zr^{4+}–O^{2-} pair in this case; the strong basic sites are associated with the low-coordination oxygen anions.[19,36] Unfortunately, attempts at deconvolution of the TPD spectrum into three peaks were unsuccessful in this case. To facilitate discussion, CO_2-TPD profiles are roughly divided into three regions:[37,38] 50–150 °C, 150–240 °C and > 240 °C, which correspond to CO_2 desorption of weak, medium and strong site, respectively. The number of different base site was evaluated by calculating the integral of each region, and the data were summarized in Table 4. It can be seen that the number of total basic sites of alkaline-earth oxides doped samples is higher than that of undoped $CuO–ZrO_2$. Moreover, the contributions of single basic site to the total basic sites was calculated and listed in Table 4. The fractions of the strong basic site increased in the order $C_{0.5}Z_{0.5}$ < $Mg_{0.05}C_{0.5}Z_{0.45}$ < $Ca_{0.05}C_{0.5}Z_{0.45}$ < $Sr_{0.05}C_{0.5}Z_{0.45}$ < $Ba_{0.05}C_{0.5}Z_{0.45}$, whereas a contrary trend was obtained for the weak basic site. As for the contributions of medium basic sites to total basic sites, no apparent change is observed for all investigated catalysts. It is noteworthy that, as shown in Fig. 4(A), the upper temperature limit of desorption profile increases progressively from $C_{0.5}Z_{0.5}$ to $Ba_{0.05}C_{0.5}Z_{0.45}$ sample, suggesting a continuous increase in the strength of strong basic sites. For instance, the CO_2 desorption over $C_{0.5}Z_{0.5}$ occurs at a temperature below 300 °C, while the desorption curve of $Ba_{0.05}C_{0.5}Z_{0.45}$ extend up to 450 °C. The variation of the strength of basic sites is related to the substitution of Zr^{4+} by the alkaline-earth cations. As stated above, the basicity of strong basic sites is originated from the low-coordination oxygen anions; the greater an oxygen anion's electrodonating is, the stronger its Lewis basicity will be.[39,40] It is well known that the electronegativity of alkaline-earth cations is smaller than that of Zr^{4+} and decreases in the order Mg^{2+} < Ca^{2+} < Sr^{2+} < Ba^{2+}. Therefore, the electrodonating property of oxygen anions neighboring Zr^{4+} enhance with the partial substitution of Zr^{4+} by alkaline-earth cations, leading to the increase in the strength of basic sites.

Fig. 4(B) shows the CO_2-TPD curves of $CuO–ZrO_2$ catalysts doped with different MgO content. The TPD curve extends to a higher temperature with increasing the amount of MgO doping, which also indicates an enhancement in the strength of strong basic sites. Furthermore, as shown in Table 4, the increase in MgO doping give rise to an increase in the fractions of the strong basic site.

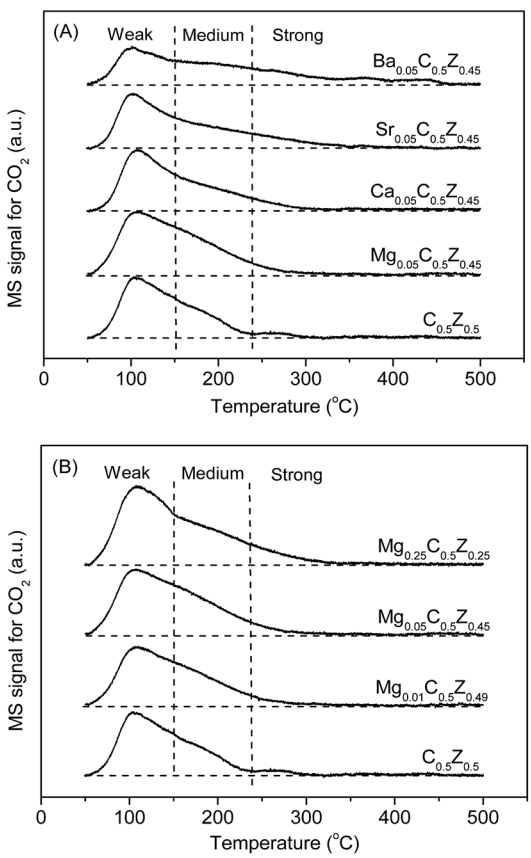

Fig. 4 CO_2-TPD profiles of $CuO–ZrO_2$ catalysts doped with different alkaline-oxide (A) and with different amount of MgO (B).

Table 4 The basicity and the distribution of basic sites over $CuO–ZrO_2$ catalysts doping with alkaline-earth oxides

	Number of basic sites (μmol g^{-1}) and contribution[a] (%)			
Catalyst	Weak	Medium	Strong	Total
$C_{0.5}Z_{0.5}$	12.6 (64.4)	6.4 (32.6)	0.6 (3.0)	19.6
$Mg_{0.05}C_{0.5}Z_{0.45}$	14.2 (58.1)	9.2 (37.6)	1.0 (4.3)	24.4
$Ca_{0.05}C_{0.5}Z_{0.45}$	12.2 (56.7)	7.7 (36.0)	1.6 (7.3)	21.5
$Sr_{0.05}C_{0.5}Z_{0.45}$	11.1 (53.6)	6.8 (33.1)	2.7 (13.3)	20.6
$Ba_{0.05}C_{0.5}Z_{0.45}$	8.0 (39.9)	6.5 (32.4)	5.6 (27.7)	20.1
$Mg_{0.01}C_{0.5}Z_{0.49}$	12.2 (59.0)	7.7 (37.4)	0.7 (3.6)	20.6
$Mg_{0.25}C_{0.5}Z_{0.25}$	16.4 (55.8)	10.4 (35.4)	2.6 (8.8)	29.4

[a] The number of weak, medium and strong sites expressed in the amount of desorbed CO_2 at 50–150, 150–240 and >240 °C, respectively. The value in the parenthesis is the fraction of single basic site to the number of total basic site.

Table 5 Catalytic performance for hydrogenation of CO_2 to methanol over $Cu–ZrO_2$ catalysts doping with alkaline-earth oxides[a]

Catalyst	CO_2 conversion (%)	CH_3OH selectivity (%)	CH_3OH yield (%)
$C_{0.5}Z_{0.5}$	9.9	45.4	4.5
$Mg_{0.05}C_{0.5}Z_{0.45}$	10.6	50.9	5.4
$Ca_{0.05}C_{0.5}Z_{0.45}$	8.1	51.5	4.2
$Sr_{0.05}C_{0.5}Z_{0.45}$	5.9	52.7	3.1
$Ba_{0.05}C_{0.5}Z_{0.45}$	5.4	40.6	2.2
$Mg_{0.01}C_{0.5}Z_{0.49}$	9.8	49.0	4.8
$Mg_{0.03}C_{0.5}Z_{0.47}$	10.3	51.5	5.3
$Mg_{0.1}C_{0.5}Z_{0.4}$	10.5	51.3	5.4
$Mg_{0.25}C_{0.5}Z_{0.25}$	8.8	47.2	4.2

[a] Experimental errors are within ±3% of the values reported. Reaction conditions: $T = 240$ °C, $P = 3.0$ MPa, GHSV = 3600 h^{-1}.

3.5 Catalytic activity and selectivity

Activity and selectivity results for methanol synthesis from CO_2 hydrogenation over the undoped and alkaline-earth oxides doped $CuO–ZrO_2$ catalysts are summarized in Table 5. Methanol and CO are the only carbon-containing products under the reaction conditions and traces of methane can be detected at high temperatures.

As illustrated in Table 5, the conversion of CO_2 declined with the incorporation of CaO, SrO and BaO, and a catalytic activity sequence of $C_{0.5}Z_{0.5}$ > $Ca_{0.05}C_{0.5}Z_{0.45}$ > $Sr_{0.05}C_{0.5}Z_{0.45}$ > $Ba_{0.05}C_{0.5}Z_{0.45}$ was obtained. However, for the MgO-doped $CuO–ZrO_2$ sample, an increase in CO_2 conversion was observed as the doping amount is no more than 10 mol%. A further increase in the doping amount of MgO results in a decrease in CO_2 conversion. As well documented, the catalytic activity and the S_{Cu} in a reduced catalyst are strongly correlated, and a large value of S_{Cu} is favorable for a high catalytic activity for the hydrogenation of CO_2.[5,12,13,41,42] Obviously, the decrease in CO_2 conversion over CaO-, SrO- and BaO-doped catalysts is contradictory to the above statement because the S_{Cu} increases significantly with the doping of alkaline-earth oxide, as shown in the part of 3.1. This can be explained as follows. According to the dual-site mechanism, the Cu component serves to dissociatively adsorb H_2 and to provide a source of atomic hydrogen by spillover. In fact, there are two steps involved in the process of dissociatively adsorb H_2. One is the adsorption of H_2 over the Cu active site; the other is the dissociation of the adsorbed H_2. The results of H_2-TPR disclosed that the reducibility of CuO was depressed with the introduction of CaO, SrO and BaO. Since the reducibility of CuO reflect the easiness of the dissociation of adsorbed H_2, the decline in the reducibility of CuO implies that the adsorbed H_2 over the resulting Cu sites become more difficult to dissociate. In other words, with the addition of CaO, SrO and BaO, the rate of producing atomic hydrogen decreases though more Cu active sites are available for H_2 adsorption. As a result, compared to the undoped $CuO–ZrO_2$ catalyst, CaO-, SrO- and BaO-doped samples exhibit a lower CO_2 conversion. Moreover, since the reducibility of CuO in catalyst decreases in a sequence of $Ca_{0.05}C_{0.5}Z_{0.45}$ > $Sr_{0.05}C_{0.5}Z_{0.45}$ > $Ba_{0.05}C_{0.5}Z_{0.45}$, the same sequence of the conversion of CO_2 is obtained. For the MgO-doped samples, a remarkable increase in the copper surface area is observed; while the effects of the doping on the reducibility of CuO is much less than that of CaO-, SrO- and BaO-doped samples, as stated in the part of 3.3. Under such a condition, the copper surface area will be a predominant factor. Therefore, it can be understood that a small increase in the CO_2 conversion is achieved when an appropriate amount of MgO is introduced into $CuO–ZrO_2$. As the amount of MgO doping is 25 mol%, the decline in the reducibility of CuO will be significant, which results in a low conversion of CO_2, and a value of 8.8% is obtained on $Mg_{0.25}C_{0.5}Z_{0.25}$ sample.

As also shown in Table 5, the methanol selectivity increases with the addition of MgO, CaO, and SrO. Various factors affecting the methanol selectivity have been proposed.[43–45] Recent investigation revealed that the surface basicity of the catalyst play a dominant role in determining the methanol selectivity, and the carbon containing intermediates adsorbed on the stronger basic site preferred to hydrogenate further to form methanol rather than dissociate to form CO.[18,19] The results of CO_2-TPD showed that both the strength and contribution of strong basic sites increased with the introduction of alkaline-earth oxides. Therefore, MgO-, CaO-, and SrO-doped samples exhibit a higher methanol selectivity comparing to the undoped $CuO–ZrO_2$. Nevertheless, the methanol selectivity decreases as BaO is incorporated into $CuO–ZrO_2$. It is possible that the decline in methanol selectivity is related to the excessive basicity of BaO-doped sample, which will lower the activation and hydrogenation of the adsorbed intermediates. As the amount of MgO doping varies from 1 to 5 mol%, the change in the methanol selectivity (49.0–51.5%) is small because the change in the surface basicity of these catalysts is not significant, as can be seen from Fig. 4(B).

Table 5 shows the methanol yield over the undoped and alkaline-earth oxides doped $CuO–ZrO_2$. The methanol yield increases with the doping of MgO, and a maximum of 5.4% was

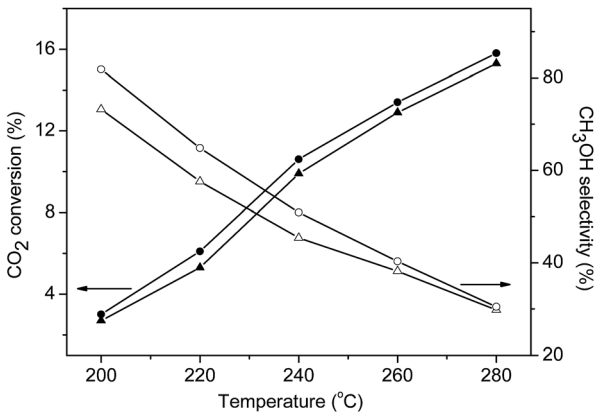

Fig. 5 Effect of temperature on the conversion of CO_2 (solid symbols) and selectivity of methanol (open symbols) over $C_{0.5}Z_{0.5}$ (triangles) and $Mg_{0.05}C_{0.5}Z_{0.45}$ (circles) catalysts. Reaction conditions: $H_2/CO_2 = 3$, $P = 3.0$ MPa, GHSV = 3600 h^{-1}.

obtained over the $Mg_{0.05}C_{0.5}Z_{0.45}$ sample. In comparison with the undoped CuO–ZrO_2, the value increased by 20%. For the CaO-, SrO-, BaO-doped samples, the methanol yield is lower than that of undoped CuO–ZrO_2 catalyst, and a sequence of $Ca_{0.05}C_{0.5}Z_{0.45}$ > $Sr_{0.05}C_{0.5}Z_{0.45}$ > $Ba_{0.05}C_{0.5}Z_{0.45}$ is obtained. Furthermore, the effects of reaction temperature on the catalytic performances were investigated over the $C_{0.5}Z_{0.5}$ and $Mg_{0.05}C_{0.5}Z_{0.45}$ catalysts. As shown in Fig. 5, with the elevation of reaction temperature, the conversion of CO_2 increases but the CH_3OH selectivity decreases. Similar results can be found in the literature.[30,33] This variation can be explained in terms of thermodynamics and kinetics. The synthesis of methanol and the reverse water-gas shift (RWGS) are the two parallel reactions involved in the CO_2 hydrogenation process. The synthesis of methanol is an exothermic reaction, whereas the reaction of RWGS exhibits endothermic character.[7,19] According to the thermodynamic principle, raising temperature is favorable for the formation of CO *via* the RWGS reaction. On the other hand, in comparison with methanol synthesis, the RWGS reaction has a higher apparent activation energy,[33,46] which means that the increase in CO production is faster than that of methanol with the increase in temperature. Consequently, the CH_3OH selectivity decreases along with the elevation of reaction temperature.

4. Conclusions

CuO–ZrO_2 catalysts doped with alkaline-earth oxides were prepared and used for methanol synthesis from CO_2 hydrogenation. The effects of alkaline-earth oxides on the physicochemical and catalytic properties of catalysts were investigated. Based on the results of this work, the following conclusions can be made:

1 The introduction of alkaline-earth oxides hinders the crystallization of CuO and ZrO_2 components in CuO–ZrO_2 catalyst and improves the copper surface area as well as the BET surface area.

2 The incorporation of alkaline-earth oxides gives rise to a decrease in the interaction between CuO and ZrO_2 and further a decline in the reducibility of CuO.

3 Both the strength and the contribution of strong basic site increase with the addition of alkaline-earth oxides.

4 The conversion of CO_2 depends not only on the copper surface area but also on the reducibility of CuO in catalyst, and the latter play a predominant role in methanol synthesis over CaO-, SrO- and BaO-doped CuO–ZrO_2 catalyst. The increase in methanol selectivity correlate with the increase in the strength and the contribution of strong basic sites.

5 A suitable amount of MgO in CuO–ZrO_2 is beneficial for the catalytic activity and methanol selectivity, and a maximum methanol yield is obtained as the content of MgO doping is 5 mol%.

Acknowledgements

The authors thank Shanghai Municipal Education Commission (no. 13YZ117), Shanghai Municipal Science and Technology Commission (no. 13ZR1441200) and the National Natural Science Foundation of China (no. 21273150) for financial support.

Notes and references

1 C. Song, *Catal. Today*, 2006, **115**, 2.
2 W. Wang, S. P. Wang, X. B. Ma and J. L. Gong, *Chem. Soc. Rev.*, 2011, **40**, 3703.
3 G. A. Olah, A. Goeppert and G. K. S. Prakash, *J. Org. Chem.*, 2009, **74**, 487.
4 X. M. Liu, G. Q. Lu and Z. F. Yan, *Appl. Catal., A*, 2005, **279**, 241.
5 F. Arena, K. Barbera, G. Italiano, G. Bonura, L. Spadaro and F. Frusteri, *J. Catal.*, 2007, **249**, 185.
6 R. A. Köppel, C. Stöcker and A. Baiker, *J. Catal.*, 1998, **179**, 515.
7 X. M. Guo, D. S. Mao, G. Z. Lu, S. Wang and G. S. Wu, *J. Catal.*, 2010, **271**, 178.
8 X. M. Guo, D. S. Mao, S. Wang, G. S. Wu and G. Z. Lu, *Catal. Commun.*, 2009, **10**, 1661.
9 R. Raudaskoski, M. V. Niemelä and R. L. Keiski, *Top. Catal.*, 2007, **45**, 57.
10 M. Kilo, J. Weigel, A. Wokaun, R. A. Köeppel, A. Stoeckli and A. Baiker, *J. Mol. Catal. A: Chem.*, 1997, **126**, 169.
11 J. Słoczyński, R. Grabowski, A. Kozłowska, P. Olszewski, M. Lachowska, J. Skrzypek and J. Stoch, *Appl. Catal., A*, 2003, **249**, 129.
12 J. Słoczyński, R. Grabowski, P. Olszewski, A. Kozłowska, J. Stoch, M. Lachowska and J. Skrzypek, *Appl. Catal., A*, 2006, **310**, 127.
13 S. Natesakhawat, J. W. Lekse, J. P. Baltrus, P. R. Ohodnicki Jr, B. H. Howard, X. Y. Deng and C. Matranga, *ACS Catal.*, 2012, **2**, 1667.
14 H. Y. Ban, C. M. Li, K. Asami and K. Fujimoto, *Catal. Commun.*, 2014, **54**, 50.
15 I. A. Fisher and A. T. Bell, *J. Catal.*, 1997, **172**, 222.
16 F. Arena, G. Italiano, K. Barbera, S. Bordiga, G. Bonura, L. Spadaro and F. Frusteri, *Appl. Catal., A*, 2008, **350**, 16.
17 Q. J. Hong and Z. P. Liu, *Surf. Sci.*, 2010, **604**, 1869.

18 X. M. Guo, D. S. Mao, G. Z. Lu, S. Wang and G. S. Wu, *J. Mol. Catal. A: Chem.*, 2011, **345**, 60.
19 P. Gao, F. Li, H. J. Zhan, N. Zhao, F. K. Xiao, W. Wei, L. S. Zhong, H. Wang and Y. H. Sun, *J. Catal.*, 2013, **298**, 51.
20 P. Gao, F. Li, N. Zhao, F. K. Xiao, W. Wei, L. S. Zhong and Y. H. Sun, *Appl. Catal., A*, 2013, **468**, 442.
21 W. Y. Zhang, H. Wang, W. Wei and Y. H. Sun, *J. Mol. Catal. A: Chem.*, 2005, **231**, 83.
22 L. M. Madeira, R. M. Martín-Aranda, F. J. Maldonado-Hódar, J. L. G. Fierro and M. F. Portela, *J. Catal.*, 1997, **169**, 469.
23 S. N. He, Y. J. Cui, Y. L. Yao, R. M. Fang, Z. H. Shi, M. C. Gong and Y. Q. Chen, *Acta Phys.-Chim. Sin.*, 2011, **27**, 1157.
24 S. R. Jain, K. C. Adiga and V. R. Pai Verneker, *Combust. Flame*, 1981, **40**, 71.
25 G. C. Chinchen, C. M. Hay, H. D. Vandervell and K. C. Waugh, *J. Catal.*, 1987, **103**, 79.
26 R. Watanabe, Y. Saito and C. Fukuhara, *Appl. Catal., A*, 2014, **482**, 344.
27 N. N. Das, J. Konar, M. K. Mohanta and S. C. Srivastava, *J. Colloid Interface Sci.*, 2004, **270**, 1.
28 F. Papa, P. Luminita, P. Osiceanu, R. Birjega, M. Akane and I. Balint, *J. Mol. Catal. A: Chem.*, 2011, **346**, 46.
29 G. Avgouropoulos, T. Ioannides and H. Matralis, *Appl. Catal., B*, 2005, **56**, 87.
30 Y. P. Zhang, J. H. Fei, Y. M. Yu and X. M. Zheng, *Energy Convers. Manage.*, 2006, **47**, 3360.
31 N. F. P. Ribeiro, M. M. V. M. Souza and M. Schmal, *J. Power Sources*, 2008, **179**, 329.
32 L. C. Wang, Q. Liu, M. Chen, Y. M. Liu, Y. Cao, H. Y. He and K. N. Fan, *J. Phys. Chem. C*, 2007, **111**, 16549.
33 I. Melián-Cabrera, M. López Granados and J. L. G. Fierro, *J. Catal.*, 2002, **210**, 273.
34 M. D. Rhodes and A. T. Bell, *J. Catal.*, 2005, **233**, 198.
35 Z. Liu, J. A. Cortés-Concepción, M. Mustian and M. D. Amiridis, *Appl. Catal., A*, 2006, **302**, 232.
36 V. K. Díez, C. R. Apesteguía and J. I. Di Cosimo, *Catal. Today*, 2000, **63**, 53.
37 S. Kuś, M. Otremba, A. Tórz and M. Taniewski, *Appl. Catal., A*, 2002, **230**, 263.
38 H. Wang, M. H. Wang, W. Y. Zhang, N. Zhao, W. Wei and Y. H. Sun, *Catal. Today*, 2006, **115**, 107.
39 H. Wang, M. H. Wang, S. G. Liu, N. Zhao, W. Wei and Y. H. Sun, *J. Mol. Catal. A: Chem.*, 2006, **258**, 308.
40 S. F. Xia, X. M. Guo, D. S. Mao, Z. P. Shi, G. S. Wu and G. Z. Lu, *RSC Adv.*, 2014, **4**, 51688.
41 M. Saito, T. Fujitani, M. Takeuchi and T. Watanabe, *Appl. Catal., A*, 1996, **138**, 311.
42 Q. Sun, Y. L. Zhang, H. Y. Chen, J. F. Deng, D. Wu and S. Y. Chen, *J. Catal.*, 1997, **167**, 92.
43 S. Fujita, S. Moribe, Y. Kanamori, M. Kakudate and N. Takezawa, *Appl. Catal., A*, 2001, **207**, 121.
44 J. Toyir, P. R. de la Piscina, J. L. G. Fierro and N. Homs, *Appl. Catal., B*, 2001, **34**, 255.
45 M. D. Rhodes and A. T. Bell, *J. Catal.*, 2005, **233**, 198.
46 J. Yoshihara and C. T. Campbell, *J. Catal.*, 1996, **161**, 776.